frontiers | Frontiers in Environmental Science

TYPE Original Research
PUBLISHED 23 November 2022
DOI 10.3389/fenvs.2022.1068155

Check for updates

OPEN ACCESS

EDITED BY
Zhiyuan Hu,
School of atmospheric sciences, Sun Yat-sen University, China

REVIEWED BY
Zhiqiang Gong,
Beijing Climate Center (BCC), China
Gen Li,
Hohai University, China

*CORRESPONDENCE
Xiangwei Kong,
xiangwei580@163.com

SPECIALTY SECTION
This article was submitted to Atmosphere and Climate, a section of the journal Frontiers in Environmental Science

RECEIVED 12 October 2022
ACCEPTED 08 November 2022
PUBLISHED 23 November 2022

CITATION
Tao W, Kong X, Liu Y, Wang Y and Dong D (2022), Diversity of Northwest Pacific atmospheric circulation anomalies during post-ENSO summer. *Front. Environ. Sci.* 10:1068155. doi: 10.3389/fenvs.2022.1068155

COPYRIGHT
© 2022 Tao, Kong, Liu, Wang and Dong. This is an open-access article distributed under the terms of the Creative Commons Attribution License (CC BY). The use, distribution or reproduction in other forums is permitted, provided the original author(s) and the copyright owner(s) are credited and that the original publication in this journal is cited, in accordance with accepted academic practice. No use, distribution or reproduction is permitted which does not comply with these terms.

Diversity of Northwest Pacific atmospheric circulation anomalies during post-ENSO summer

Weichen Tao[1], Xiangwei Kong[2]*, Yong Liu[3], Ya Wang[1] and Danhong Dong[1]

[1]State Key Laboratory of Numerical Modeling for Atmospheric Sciences and Geophysical Fluid Dynamics, Institute of Atmospheric Physics, Chinese Academy of Sciences, Beijing, China, [2]Lanzhou Central Meteorological Observatory, Lanzhou, China, [3]Center for Monsoon System Research, Institute of Atmospheric Physics, Chinese Academy of Sciences, Beijing, China

In present study, the diversity of summertime Northwest Pacific (NWP) atmospheric circulation anomalies following El Niño-Southern Oscillation is investigated by performing the inter-case empirical orthogonal function (EOF) analysis among 33 El Niño cases and 36 La Niña cases, respectively. Although an anomalous anticyclone is observed over the NWP for all El Niño cases' composite, the circulation anomalies there vary from one case to another for each case. The EOF1 mode of NWP circulation anomalies explains 39.8% of inter-case variance, and its positive phase features an anomalous anticyclone and cyclone at south and north of 25°N, respectively. Therefore, the positive first principal component (PC1) corresponds to the anomalous NWP anticyclone, while the anticyclone shifts more northeastward and a cyclone appears at its south side for negative PC1. The PC1-related NWP circulation anomalies are largely controlled by the pronounced central and eastern Pacific sea surface temperature cooling, which indicates the diverse El Niño decay rate. Furthermore, four categories are obtained according to the El Niño decay rate by the nonlinear k-means cluster analysis, and the results further confirm that the close relationship between NWP circulation anomalies and El Niño decay rate. The PC1-regressed land rainfall anomalies highly resembles the composite results in the key areas of Asian monsoon region: the central China and South Asia, indicating variable rainfall anomalies in these areas during post-El Niño summer. The conclusion obtained from La Niña cases are generally same to El Niño.

KEYWORDS

post-ENSO summer, ENSO decay rate, Northwest Pacific circulation, k-means cluster analysis, Asian monsoon rainfall

1 Introduction

El Niño-Southern Oscillation (ENSO) is a dominant mode of tropical interannual variability and exerts great influence on global climate (e.g., Lau and Nath 1996; Webster et al., 1998; Trenberth et al., 2002). During El Niño/La Niña decaying summer, an anomalous lower-tropospheric anticyclone/cyclone often appears over the Northwest Pacific (NWP; Fu and Ye 1988; Lau 1992; Zhang et al., 1996), and strongly influences the climate of Asian monsoon region, where accounts for more than half of the world's population. Specifically, the El Niño-induced anomalous NWP anticyclone (NWPAC) weakens NWP summer monsoon by suppressing local convection (Wang et al., 2000; Wu et al., 2010; Xiang et al., 2013), enhancing dry anomalies and anomalous downward vertical motions, which reduce the NWP tropical cyclone number (Du et al., 2011) and lead to the extreme warm summer in southern China (Hu et al., 2011; Hu et al., 2012). While the moisture transport from tropics to East Asia is strengthened, rainfall over the mountainous central China is significantly enhanced due to orographic lifting (Wu et al., 2003; Hu et al., 2017; Hu et al., 2020). Moreover, a tripole pattern of precipitation anomalies over the South Asian region can be observed when the anomalous anticyclone extends westward to the North Indian Ocean (Mishra et al., 2012; Chowdary et al., 2016a; Srinivas et al., 2018; Chowdary et al., 2019; Liu and Huang 2019; Tang et al., 2022b), characterizing a prolonged hot pre-monsoon period and a delay of the South Asian summer monsoon onset (Zhou et al., 2019). These climate responses are nearly reversed during La Niña, although the asymmetry exists between El Niño and La Niña (e.g., Hoerling et al., 1997; Hoerling et al., 2001; Zhang et al., 2014; Tao et al., 2017; Wang et al., 2021b; Wang et al., 2022). Thus, the anomalous atmospheric circulation over the NWP plays a crucial role in linking ENSO and Asian climate.

During the summer following El Niño, the NWPAC is maintained by local cooling *via* a positive thermodynamic feedback between SST and circulation anomalies (Wang et al., 2000; Wang and Zhang 2002; Wang et al., 2013; Xiang et al., 2013; Gong et al., 2018a) and remote tropical Indian Ocean warming (TIO) *via* Kelvin wave induced Ekman divergence mechanism (Yang et al., 2007; Wu et al., 2009; Xie et al., 2009; Yang et al., 2010; Hu et al., 2014; Tao et al., 2015). The NWP cooling and TIO warming can serve as the Indo-western Pacific Ocean capacitor (IPOC) mode to anchor the NWPAC (Xie et al., 2016; Xie and Zhou 2017; Hu et al., 2019). However, the response of summertime NWP circulation following ENSO is not stable. It varies from one ENSO case to another (Chowdary et al., 2016a; Chowdary et al., 2016b; Chen et al., 2016; Chen et al., 2017; Tao et al., 2017; Wang et al., 2017; Tao et al., 2018; Jiang et al., 2019; Li et al., 2019; Tao et al., 2019), and is subject to ENSO-unrelated (internal) variability (Kosaka et al., 2013; Li et al., 2016; Gong et al., 2018b; Wang et al., 2018; Zhou et al., 2018; Wang et al., 2020b; Chen et al., 2020; Wang et al., 2020c). As a result, a robust rainfall response to ENSO has not been fully recognized outside the Asian monsoon researchers, as shown by the schematic diagrams of ENSO impacts on the web pages of National Oceanic and Atmospheric Administration (NOAA), International Research Institute for Climate and Society (IRI), Met Office, and so on. The pronounced rainfall anomalies in summer seem to develop only after a strong ENSO (Wang et al., 2017), leading to the most severe forecast errors during ENSO decay phase (Ham et al., 2019; Wang et al., 2020a). In present study, the diversity of NWP circulation anomalies during post-ENSO summer is explored by using inter-case empirical orthogonal function (EOF) analysis, founding that the diverse circulation anomalies tend to cause the variable rainfall response in the key areas of East and South Asia, i.e., the mountainous central China (Hu et al., 2017; Hu et al., 2020) and western India (Chowdary et al., 2019). The rest of the paper is organized as follows. Section 2 describes the data and methods. The main results are presented in Section 3, followed by the conclusion and discussion in Section 4.

2 Data and methods

The atmospheric variables are derived by averaging two merged reanalysis datasets, one from the National Centers for Environmental Prediction/National Center for Atmospheric Research (NCEP/NCAR) and the other from the European Centre for Medium-Range Weather Forecasts (ECMWF). The NOAA-Cooperative Institute for Research in Environmental Sciences Twentieth Century Reanalysis V2c (20CR; Compo et al., 2011) and NCEP-US Department of Energy Atmospheric Model Inter-comparison Project II reanalysis (NCEP2; Kanamitsu et al., 2002) are combined into a merged NCEP dataset. The merged ECMWF dataset is made from ECMWF twentieth century reanalysis (ERA20C; Poli et al., 2016) and fifth generation reanalysis (ERA5; Hersbach et al., 2020). To ensure temporal consistency, the mean states of 20CR (ERA20C) and NCEP2 (ERA5) are calibrated by removing their differences during the overlap period 1979–2015 (1979–2010). The monthly mean SST dataset used is made by averaging the Hadley Centre Sea ICE and SST (HadISST; Rayner and Coauthors, 2003) and NOAA Extended Reconstructed SST (ERSST; Smith and Reynolds, 2003) V5 datasets. The monthly mean land precipitation dataset is merged by the Climatic Research Unit (CRU) TS4.01 (Harris et al., 2014) and Global Precipitation Climatology Centre (GPCC) V7 (Schneider et al., 2014) datasets. The above merged datasets are used to get long-term and reliable data record, and the period from 1901 to 2017 are selected for analysis.

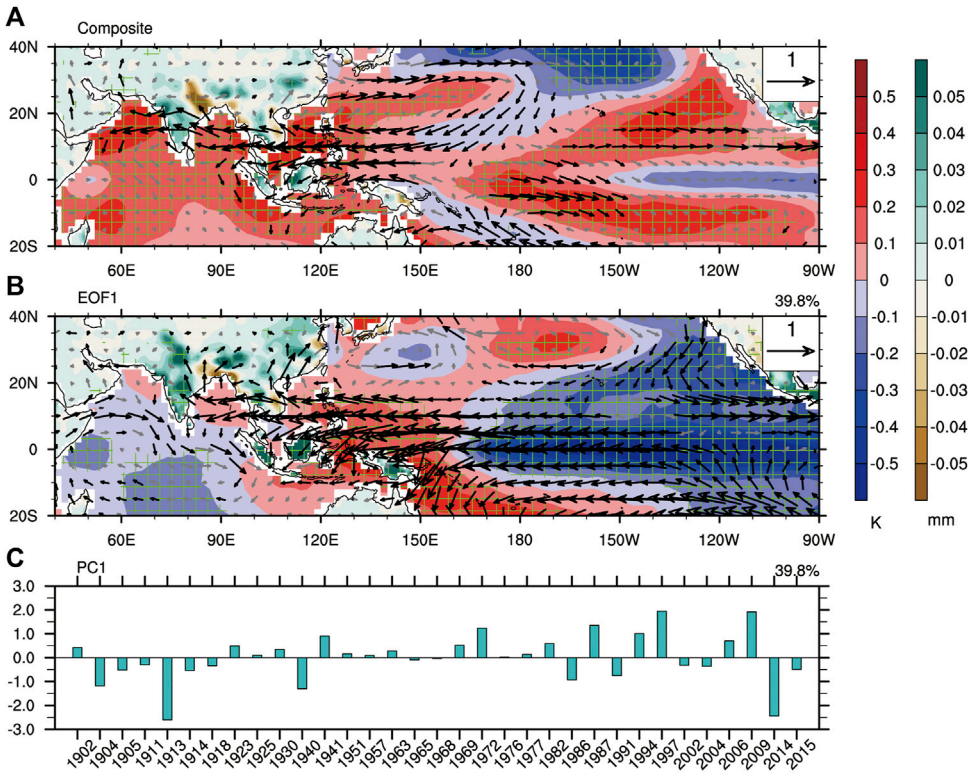

FIGURE 1
(A) Composite anomalies of SST (shaded over the ocean; °C), 850-hPa winds (vectors; m s^{-1}), and precipitation (shaded over the land; mm) during post El Niño summer for 33 El Niño cases. **(B)** Regression of SST (shaded over the ocean; °C), 850-hPa winds (vectors; m s^{-1}), and precipitation (shaded over the land; mm) with respect to **(C)** the standardized PC1 of 850-hPa wind anomalies over the NWP (0°–40°N, 100°E–180°) during post El Niño summer for 33 El Niño cases. Green lattices and black vectors indicate that the confidence level reaches 90%. The EOF1 explained variance fractions are given at the top right of **(B)** and **(C)**.

The monthly mean climatology is first calculated for the 1901–2017 period, and monthly anomalies are then computed as the departure from the climatology. Besides, the linear trend has been removed from all datasets. The Niño3.4 index is defined as SST anomalies averaged over the central and eastern equatorial Pacific (CEP, 5°S–5°N, 170°–120°W). Hereafter, any month in ENSO onset and decay year is denoted by the suffix (0) and (1), respectively. Consistent with Wang et al. (2019) and Wang et al. (2020a), an El Niño (La Niña) year is identified as that the Niño3.4 index during October-November-December(0)-January-February(1) is greater (less) than or equals to 0.6°C (−0.5°C). As a result, 33 El Niño cases and 36 La Niña cases are identified. Only the results of El Niño are shown in the main text, and the results of La Niña are given in the supplemental material and briefly discussed in last section. EOF, regression, correlation, k-means cluster, and composite analysis are used, and the confidence level is estimated based on the standard two-tailed Student's *t*-test. The k-means cluster analysis is introduced on the first occasion that it is used.

3 Results

3.1 Inter-case EOF of NWPAC during post-ENSO summer

Figure 1A shows the composite SST, 850-hPa winds, and land precipitation during post-El Niño summer for 33 El Niño cases. The most significant feature of atmospheric circulation anomalies averaged for all cases is an anomalous anticyclone over the NWP, and the easterly wind anomalies at the south flank of NWPAC extend westward to the north Indian Ocean (Figure 1A). As that the El Niño-related CEP warming gradually decays, the NWPAC is mainly anchored by IPOC mode with TIO warming and NWP cooling (Xie et al., 2016; Xie and Zhou 2017).

The NWP circulation anomalies during post-El Niño summer vary from one case to another (Supplementary Figure S1). To reveal the possible factor responsible for the diversity of NWP circulation anomalies among 33 El Niño cases, an inter-case EOF analysis is applied to the 850-hPa wind anomalies over

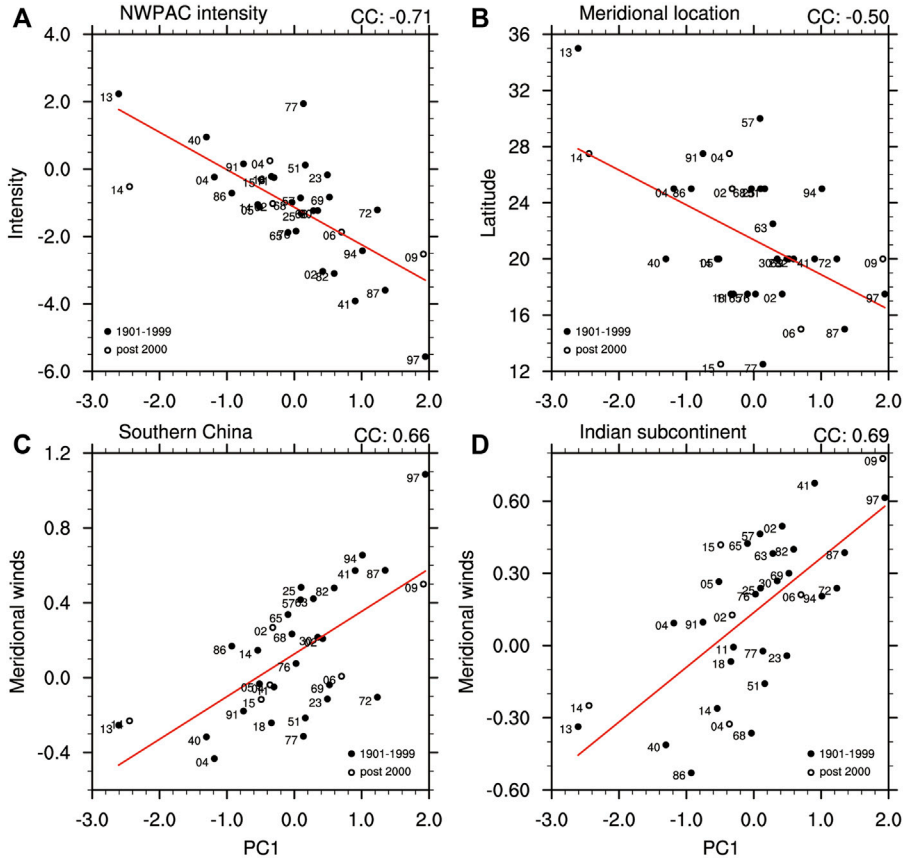

FIGURE 2
Scatter diagram of standardized PC1 and **(A)** NWPAC intensity, **(B)** meridional location of NWPAC center, **(C)** 850-hPa meridional wind anomalies over the southern China (15°–30°N, 100°–110°E), and **(D)** 850-hPa meridional wind anomalies over the India subcontinent (15°–30°N, 80°–90°E) in 33 El Niño cases. The meridional location of NWPAC center is determined by the maximum value of anomalous 850-hPa stream function over the NWP (10°–45°N, 100°–170°E) as shown by red dots in Supplementary Figure S1. The red lines denote the best fit lines for 33 El Niño cases, and the correlation coefficients are on the top-right corner of each figure.

the NWP region (0°–40°N, 100°E–180°). EOF1 mode explains 39.8% of total inter-case variance and is well separated with other modes (Figures 1B,C). The positive EOF1 phase is characterized by a meridional dipole pattern of circulation anomalies with an anomalous anticyclone and cyclone located at south and north of 25°N over the NWP, respectively (Figure 1B). Therefore, the positive first principal component (PC1) value corresponds to the NWPAC, while the anticyclone shifts more northeastward and an anomalous cyclone appears over the NWP for negative PC1 value.

Furthermore, PC1 has a close relationship with the intensity (Figure 2A), meridional (Figure 2B), and zonal location (Figures 2C,D) of NWPAC. The intensity of NWP circulation anomalies is defined as the difference of 850 hPa zonal winds between a southern region (5°–15°N, 90°–30°E) and a northern region (22.5°–32.5°N, 110°–140°E) following Wang and Fan (1999), and the NWPAC intensity is negative. If the NWPAC shifts northeastward and an anomalous cyclone appears at its South side, a positive value will appear for instead. Thus, the intensity of NWP circulation anomalies reflects the location of NWPAC indirectly. The meridional wind anomalies over the Indian subcontinent and southern China are used to represent the zonal location of NWPAC due to its east-west flat shape, which is in favor of the conversion of kinetic energy from the mean flow to perturbations (Hu et al., 2019; Wang et al., 2021a; Tang et al., 2022a). Therefore, the EOF1 mode indicates diverse location of NWPACs in 33 El Niño cases, the NWPAC shifts more northeastward as a decrease of PC1 value.

3.2 Diverse ENSO decay pace

Pronounced CEP cooling and western Pacific warming are observed in PC1-regressed SST anomalies, and the PC1-related NWPAC is a direct Rossby wave response to CEP cooling (Figure 1B; Fan et al., 2013; Wang et al., 2013; Chen et al.,

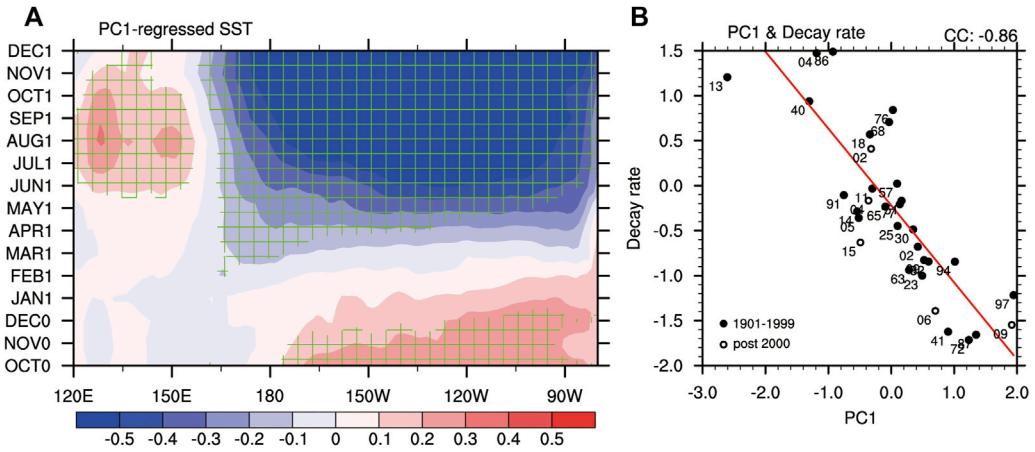

FIGURE 3
(A) Regression of SST (°C) with respect to the standardized PC1, averaged over 5°S–5°N as a function of longitude and calendar month. Green lattices indicate that the confidence level reaches 90%. **(B)** Scatter diagram of standardized PC1 and El Niño decay rate in 33 El Niño cases. El Niño decay rate is defined as the SST anomalies over the CEP (5°S–5°N, 150°–130°W) during SON(1).

2017; Tao et al., 2017; Dong et al., 2018; Tao et al., 2021). The dipole SST pattern in Pacific indicates the diverse decay pace among 33 El Niño cases. Figure 3A presents the PC1-regressed SST anomalies, averaged over 5°S–5°N as a function of longitude and calendar month. The discrepancy of CEP SST anomalies during the decay phase of 33 El Niño cases gradually increases and stabilizes after August (Figure 3A). The SST anomalies averaged over the CEP (5°S–5°N, 150°–130°W) during SON(1) season are defined as El Niño decay rate, which are highly correlated with PC1 at −0.86 reaching 99% confidence level (Figure 3B). Besides, the El Niño decay rate is significantly correlated with NWPAC intensity, central latitude, meridional wind anomalies over the southern China and Indian subcontinent at 0.55, 0.48, −0.52, and −0.69, respectively (Supplementary Figure S2), indicating that the contribution of diverse El Niño decay pace to the variable NWP circulation response.

Above study is analyzed from the perspective of circulation diversity, and the following analysis is conducted from the perspective of SST diversity to further confirm the importance of El Niño decay pace by an objective method: nonlinear k-means cluster analysis, which is more objective than directly using the El Niño decay rate with some subjective criterions. The 33 El Niño cases can be divided into four categories by a nonlinear k-means cluster analysis of the equatorial SST anomalies averaged between 5°S and 5°N over the Pacific from October(0) to October(1), following Wang et al. (2020a). The results of k-means cluster analysis depend on the number, k, of clusters chosen. k = 4 is used based on physical consideration, and other solutions of the k from two to six have been tested. The four clusters are well separated with each other according to the corresponding silhouette values (Supplementary Figure S3A), representing early decay, late decay, slow decay, and continuing cluster. Early and late decay cluster feature a fast transition to La Niña in spring and summer, respectively (Supplementary Figures S3B,C), and slow decay cluster reaches a neutral condition in subsequent winter (Supplementary Figure S3D). For continuing cluster, the CEP warming persists, and an El Niño event re-emerges in the following year (Supplementary Figure S3E). The main ocean dynamical processes for four clusters have been explored in detail by Wang et al. (2020a) through heat budget analysis.

Figure 4 shows the composite anomalies during JJA(1) for four clusters of 33 El Niño cases. Distinctive SST anomalies are observed in four types of El Niño decay, leading to the different NWP circulation response. The NWPAC in early decay cluster is maintained by a combined effect of TIO warming and CEP cooling, which trigger an eastward Kelvin wave and a westward Rossby wave, respectively (Figure 4A; Chen et al., 2016; Hu et al., 2020). In late decay cluster, the CEP cooling is not well established during JJA(1), and the NWPAC is anchored by IPOC mode, which corresponds to the zonal SST dipole with the TIO warming and NWP cooling (Figure 4B; Wang et al., 2013; Xie et al., 2016; Xie and Zhou 2017). For slow decay cluster, the CEP warming is persistent, with the NWPAC shifted northeastward and cyclonic wind anomalies appearing at the southwest side of the anticyclone (Figure 4C; Chen et al., 2017; Tao et al., 2017; Jiang et al., 2019). The dipole pattern of circulation anomalies is more distinct in continuing cluster, and the NWPAC is displaced further northeastward (Figure 4D). The CEP warming forces the cyclonic wind anomalies over the western Pacific as a Rossby wave response, leading to the lower-level divergence and suppressing the convection around the NWP. The resultant dry anomalies

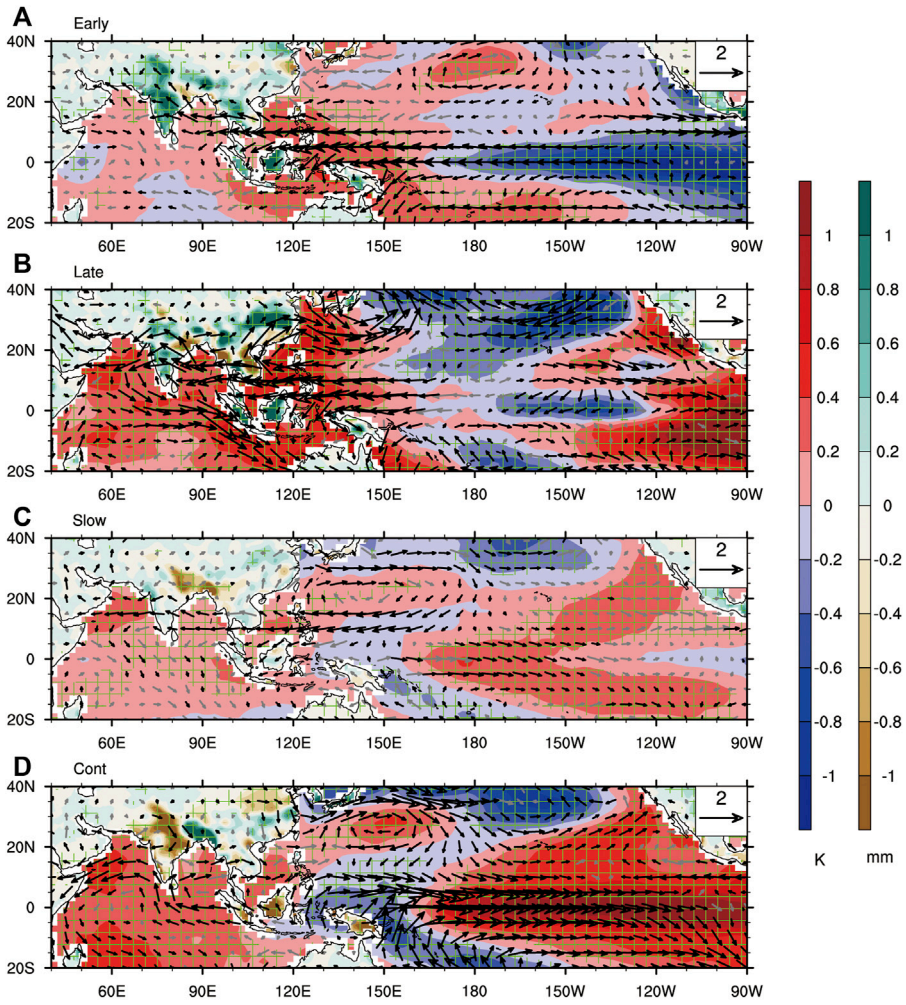

FIGURE 4
Composite anomalies of SST (shaded over the ocean; °C), 850-hPa winds (vectors; m s^{-1}), and precipitation (shaded over the land; mm) during post El Niño summer for **(A)** early decay cluster, **(B)** late decay cluster, **(C)** slow decay cluster, and **(D)** continuing cluster of 33 El Niño cases. Green lattices and black vectors indicate that the confidence level reaches 90%.

further trigger and maintain the NWPAC through the Rossby wave-induced convergence mechanism or local meridional circulation (Chen et al., 2017; Tao et al., 2017; Jiang et al., 2019). Thus, the results depicted by the four clusters confirm that the NWP circulation anomalies are largely controlled by El Niño decay pace, and the NWPAC tends to shift northeastward (southwestward) in response to slow (fast) decay rate.

3.3 Variable rainfall response in the key areas

A natural question arises, how does Asian monsoon rainfall respond to the diverse NWP circulation anomalies? Previous studies find that the enhanced rainfall over the mountainous central China (Wu et al., 2003; Hu et al., 2017; Hu et al., 2020) and a tripole rainfall pattern over the South Asian region (Mishra et al., 2012; Chowdary et al., 2016a; Srinivas et al., 2018; Chowdary et al., 2019) are induced during post-El Niño summer, as confirmed in Figure 1A. The PC1-regressed land rainfall anomalies over the Asian monsoon region highly resemble the composite anomalies, especially in the central China and South Asia (Figure 1B), and the result indicates variable rainfall response in the above-mentioned key areas. Note that the positive regressed rainfall anomalies over the central China and western India cover larger areas than the composite anomalies, and extend to the northern China and the southwest side of Tibetan Plateau, respectively.

The composite results in the four clusters further confirm the variable rainfall response to the diverse NWP circulation

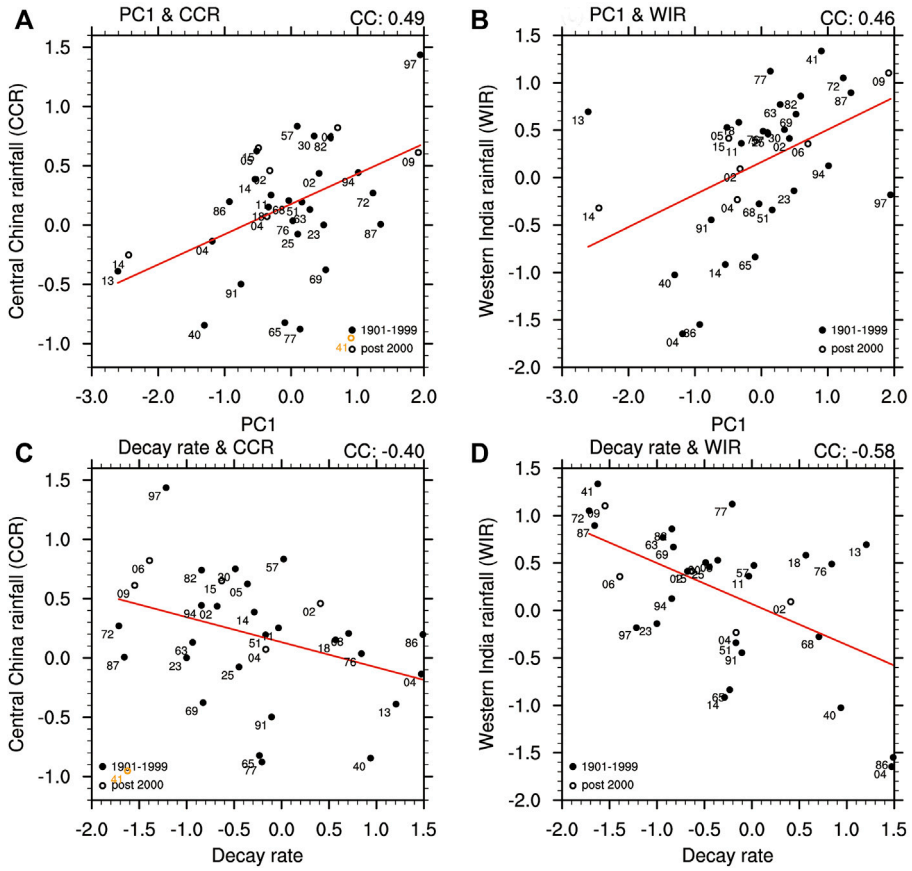

FIGURE 5
Scatter diagram of standardized PC1 and precipitation anomalies over **(A)** the central China (27.5°–37.5°N, 105°–115°E) and **(B)** the western India (8°–32°N, 70°–80°E). **(C)** and **(D)** are as **(A)** and **(B)**, but for El Niño decay rate and precipitation anomalies. The yellow dot and number represent the case is not used in calculating the best fit lines and correlation coefficients.

anomalies. The positive rainfall anomalies appear over the northern China in early decay cluster (Figure 4A). In late decay cluster, pronounced wet anomalies can be seen over the central China (Figure 4B), and the wet anomalies weaken in slow decay cluster (Figure 4C). The rainfall anomalies in continuing cluster exhibit a dipole pattern corresponding with dry and wet anomalies in the North and South of central China, respectively (Figure 4D). The tripole rainfall pattern over the South Asian region is gradually reversed from early decay cluster to continuing cluster, especially for the rainfall anomalies over the western India (Figures 4A–D). Furthermore, Figure 5 shows the scatter diagram of PC1/El Niño decay rate and rainfall anomalies in the key areas: the central China (27.5°–37.5°N, 105°–115°E) and western India (8°–32°N, 70°–80°E). Indeed, PC1 and El Niño decay rate are significantly correlated with rainfall anomalies, documenting that the diversity of El Niño decay pace leads to the variable rainfall response in the key areas of Asian monsoon region through diverse NWPAC.

4 Conclusion and discussion

The diversity of summertime NWP circulation anomalies in response to ENSO decay pace is investigated in present study. For post-El Niño summer, the NWP circulation anomalies vary from one case to another, and an anomalous anticyclone is observed for all cases' composite. The EOF1 mode of NWP circulation anomalies following 33 El Niño cases, explaining 39.8% of total inter-case variance, features an anomalous anticyclone and cyclone at south and north of 25°N, respectively. Therefore, the positive PC1 value corresponds to the NWPAC, while the anticyclone shifts more northeastward and an anomalous cyclone appears over the NWP for negative PC1 value.

The PC1-regressed SST anomalies show a pronounced CEP cooling during El Niño decay phase, which triggers the PC1-related NWPAC as a Rossby wave response. The CEP cooling lasts from March through August and beyond, and indicates the diverse El Niño decay rate among individual cases. A nonlinear k-means cluster analysis reveals that the NWP circulation anomalies are largely

controlled by El Niño decay pace, and the NWPAC tends to shift northeastward (southwestward) in response to slow (fast) decay rate. The land rainfall anomalies respond to the diverse NWP circulation anomalies highly resemble the composite rainfall anomalies in the key areas of Asian monsoon region: the central China and South Asia, indicating variable rainfall response in these areas.

An inter-case EOF analysis is also performed for NWP circulation anomalies in 36 La Niña cases (Supplementary Figure S4). The conclusion obtained from La Niña cases are generally same to El Niño (Supplementary Figures S4–S8), and the slow (fast) decay rate corresponds to the northeastward (southwestward) shift of NWP cyclone. The PC1-regressed CEP warming pattern and its center for La Niña cases are slightly more westward than CEP cooling for El Niño cases, as well as the circulation anomalies (Figures 1B, 3A; Supplementary Figures S4B, S6A). As a result, the rainfall response is more variable and covers larger areas over the central China and India.

The present study emphasizes the crucial role of ENSO decay rate to the diversity of NWP circulation anomalies and variable rainfall response, but it does not mean the lack of influence of SST anomalies in the other basins, i.e., the TIO and NWP. As shown in Figure 4 and Supplementary Figure S7, the NWP circulation anomalies in the four clusters are often maintained by the combined effect of SST anomalies in several basins. Besides, the ENSO decay rate is an important factor modulating Asian monsoon rainfall following ENSO. However, there are still large uncertainties in the prediction of ENSO, especially during its decay phase (Tippett et al., 2012; Wang et al., 2020a), and much work deserves to be done to improve ENSO forecasts.

Data availability statement

The 20CR reanalysis datasets is available at https://psl.noaa.gov/data/gridded/data.20thC_ReanV2c.html. The NCEP2 reanalysis datasets is available at https://psl.noaa.gov/data/gridded/data.ncep.reanalysis2.html. The ERA20C reanalysis datasets can be accessed from https://www.ecmwf.int/en/forecasts/datasets/reanalysis-datasets/era-20c. The ERA5 reanalysis datasets can be accessed from https://www.ecmwf.int/en/forecasts/datasets/reanalysis-datasets/era5. The ERSST dataset is obtained from https://psl.noaa.gov/data/gridded/data.noaa.ersst.v5.html. The CRU land precipitation dataset is provided at https://crudata.uea.ac.uk/cru/data/hrg/cru_ts_4.01/. The GPCC land precipitation dataset is provided at https://psl.noaa.gov/data/gridded/data.gpcc.html. The datasets generated and/or analyzed during the current study are available upon reasonable request from the authors.

Author contributions

WT and XK designed the study. WT collected the data, performed the analysis, and wrote the initial manuscript. XK, YL, YW, and DD contributed to improving the analysis and interpretation. All authors discussed and revised the manuscript.

Funding

This work was supported by the National Natural Science Foundation of China (42005132 and 42175049).

Conflict of interest

The authors declare that the research was conducted in the absence of any commercial or financial relationships that could be construed as a potential conflict of interest.

Publisher's note

All claims expressed in this article are solely those of the authors and do not necessarily represent those of their affiliated organizations, or those of the publisher, the editors and the reviewers. Any product that may be evaluated in this article, or claim that may be made by its manufacturer, is not guaranteed or endorsed by the publisher.

Supplementary material

The Supplementary Material for this article can be found online at: https://www.frontiersin.org/articles/10.3389/fenvs.2022.1068155/full#supplementary-material

References

Chen, J., Yu, J.-Y., Wang, X., and Lian, T. (2020). Different influences of southeastern Indian ocean and western Indian ocean SST anomalies on eastern China rainfall during the decaying summer of the 2015/16 extreme El Niño. *J. Clim.* 33, 5427–5443. doi:10.1175/jcli-d-19-0777.1

Chen, Z., Wen, Z., Wu, R., and Du, Y. (2017). Roles of tropical SST anomalies in modulating the Western north Pacific anomalous cyclone during strong La Niña decaying years. *Clim. Dyn.* 49, 633–647. doi:10.1007/s00382-016-3364-4

Chen, Z., Wen, Z., Wu, R., Lin, X., and Wang, J. (2016). Relative importance of tropical SST anomalies in maintaining the Western North Pacific anomalous anticyclone during El Niño to La Niña transition years. *Clim. Dyn.* 46, 1027–1041. doi:10.1007/s00382-015-2630-1

Chowdary, J. S., Harsha, H. S., Gnanaseelan, C., Srinivas, G., Parekh, A., Pillai, P., et al. (2016a). Indian summer monsoon rainfall variability in response to differences in the decay phase of El Niño. *Clim. Dyn.* 48, 2707–2727. doi:10.1007/s00382-016-3233-1

Chowdary, J. S., Parekh, A., Kakatkar, R., Gnanaseelan, C., Srinivas, G., Singh, P., et al. (2016b). Tropical Indian Ocean response to the decay phase of El Niño in a coupled model and associated changes in south and east-Asian summer monsoon circulation and rainfall. *Clim. Dyn.* 47, 831–844. doi:10.1007/s00382-015-2874-9

Chowdary, J. S., Patekar, D., Srinivas, G., Gnanaseelan, C., and Parekh, A. (2019). Impact of the indo-western Pacific Ocean capacitor mode on south Asian summer monsoon rainfall. *Clim. Dyn.* 53, 2327–2338. doi:10.1007/s00382-019-04850-w

Compo, G. P., Whitaker, J. S., Sardeshmukh, P. D., Matsui, N., Allan, R. J., Yin, X., et al. (2011). The twentieth century reanalysis Project. *Q. J. R. Meteorol. Soc.* 137, 1–28. doi:10.1002/qj.776

Dong, D., Huang, G., Tao, W., Wu, R., Hu, K., and Li, C. (2018). Interannual variation of precipitation over the Hengduan Mountains during rainy season. *Int. J. Climatol.* 38, 2112–2125. doi:10.1002/joc.5321

Du, Y., Yang, L., and Xie, S. P. (2011). Tropical Indian ocean influence on northwest Pacific tropical cyclones in summer following strong El nino. *J. Clim.* 24, 315–322. doi:10.1175/2010jcli3890.1

Fan, L., Shin, S.-I., Liu, Q., and Liu, Z. (2013). Relative importance of tropical SST anomalies in forcing East Asian summer monsoon circulation. *Geophys. Res. Lett.* 40, 2471–2477. doi:10.1002/grl.50494

Fu, C., and Ye, D. (1988). The tropical very low-frequency oscillation on interannual scale. *Adv. Atmos. Sci.* 5, 369–388. doi:10.1007/BF02656760

Gong, H., Wang, L., Chen, W., Wu, R., Huang, G., and Nath, D. (2018a). Diversity of the pacific–Japan pattern among CMIP5 models: Role of SST anomalies and atmospheric mean flow. *J. Clim.* 31, 6857–6877. doi:10.1175/jcli-d-17-0541.1

Gong, Z., Feng, G., Dogar, M. M., and Huang, G. (2018b). The possible physical mechanism for the EAP–SR co-action. *Clim. Dyn.* 51, 1499–1516. doi:10.1007/s00382-017-3967-4

Ham, Y.-G., Kim, J.-H., and Luo, J.-J. (2019). Deep learning for multi-year ENSO forecasts. *Nature* 573, 568–572. doi:10.1038/s41586-019-1559-7

Harris, I., Jones, P. D., Osborn, T. J., and Lister, D. H. (2014). Updated high-resolution grids of monthly climatic observations – The CRU TS3.10 dataset. *Int. J. Climatol.*, 34, 623–642. doi:10.1002/joc.3711

Hersbach, H., Bell, B., Berrisford, P., Hirahara, S., Horanyi, A., Munoz-Sabater, J., et al. (2020). The ERA5 global reanalysis. *Q. J. R. Meteorol. Soc.* 146, 1999–2049. doi:10.1002/qj.3803

Hoerling, M. P., Kumar, A., and Xu, T. (2001). Robustness of the nonlinear climate response to ENSO's extreme phases. *J. Clim.* 14, 1277–1293. doi:10.1175/1520-0442(2001)014<1277:rotncr>2.0.co;2

Hoerling, M. P., Kumar, A., and Zhong, M. (1997). El Niño, La Niña, and the nonlinearity of their teleconnections. *J. Clim.* 10, 1769–1786. doi:10.1175/1520-0442(1997)010<1769:enolna>2.0.co;2

Hu, K., Huang, G., and Huang, R. (2011). The impact of tropical Indian Ocean variability on summer surface air temperature in China. *J. Clim.* 24, 5365–5377. doi:10.1175/2011jcli4152.1

Hu, K., Huang, G., Qu, X., and Huang, R. (2012). The impact of Indian Ocean variability on high temperature extremes across the southern Yangtze River valley in late summer. *Adv. Atmos. Sci.* 29, 91–100. doi:10.1007/s00376-011-0209-2

Hu, K., Huang, G., Xie, S.-P., and Long, S.-M. (2019). Effect of the mean flow on the anomalous anticyclone over the Indo-Northwest Pacific in post-El Niño summers. *Clim. Dyn.* 53, 5725–5741. doi:10.1007/s00382-019-04893-z

Hu, K., Huang, G., Zheng, X.-T., Xie, S.-P., Qu, X., Du, Y., et al. (2014). Interdecadal variations in ENSO influences on northwest Pacific–east asian early summertime climate simulated in CMIP5 models. *J. Clim.* 27, 5982–5998. doi:10.1175/jcli-d-13-00268.1

Hu, K., Liu, Y., Huang, G., He, Z., and Long, S.-M. (2020). Contributions to the interannual summer rainfall variability in the mountainous area of central China and their decadal changes. *Adv. Atmos. Sci.* 37, 259–268. doi:10.1007/s00376-019-9099-5

Hu, K., Xie, S.-P., and Huang, G. (2017). Orographically anchored El Niño effect on summer rainfall in central China. *J. Clim.* 30, 10037–10045. doi:10.1175/jcli-d-17-0312.1

Jiang, W., Huang, G., Huang, P., Wu, R., Hu, K., and Chen, W. (2019). Northwest Pacific anticyclonic anomalies during post–el Niño summers determined by the pace of El Niño decay. *J. Clim.* 32, 3487–3503. doi:10.1175/jcli-d-18-0793.1

Kanamitsu, M., Ebisuzaki, W., Woollen, J., Yang, S.-K., Hnilo, J. J., Fiorino, M., et al. (2002). NCEP–DOE AMIP-II reanalysis (R-2). *Bull. Am. Meteorol. Soc.* 83, 1631–1644. doi:10.1175/bams-83-11-1631

Kosaka, Y., Xie, S. P., Lau, N. C., and Vecchi, G. A. (2013). Origin of seasonal predictability for summer climate over the Northwestern Pacific. *Proc. Natl. Acad. Sci. U. S. A.* 110, 7574–7579. doi:10.1073/pnas.1215582110

Lau, K. M. (1992). East asian summer monsoon rainfall variability and climate teleconnection. *J. Meteorological Soc. Jpn.* 70, 211–242. doi:10.2151/jmsj1965.70.1B_211

Lau, N. C., and Nath, M. J. (1996). The role of the"Atmospheric bridge" in linking tropical pacific ENSO events to extratropical SST anomalies. *J. Clim.* 9, 2036–2057. doi:10.1175/1520-0442(1996)009<2036:trotbi>2.0.co;2

Li, C., Lu, R., and Dong, B. (2016). Interdecadal changes on the seasonal prediction of the Western North Pacific summer climate around the late 1970s and early 1990s. *Clim. Dyn.* 46, 2435–2448. doi:10.1007/s00382-015-2711-1

Li, G., Jian, Y., Yang, S., Du, Y., Wang, Z., Li, Z., et al. (2019). Effect of excessive equatorial Pacific cold tongue bias on the El Niño-Northwest Pacific summer monsoon relationship in CMIP5 multi-model ensemble. *Clim. Dyn.* 52, 6195–6212. doi:10.1007/s00382-018-4504-9

Liu, Y., and Huang, R. (2019). Linkages between the south and east asian monsoon water vapor transport during boreal summer. *J. Clim.* 32, 4509–4524. doi:10.1175/jcli-d-18-0498.1

Mishra, V., Smoliak, B. V., Lettenmaier, D. P., and Wallace, J. M. (2012). A prominent pattern of year-to-year variability in Indian Summer Monsoon Rainfall. *Proc. Natl. Acad. Sci. U. S. A.* 109, 7213–7217. doi:10.1073/pnas.1119150109

Poli, P., Hersbach, H., Dee, D. P., Berrisford, P., Simmons, A. J., Vitart, F., et al. (2016). ERA-20C: An atmospheric reanalysis of the twentieth century. *J. Clim.* 29, 4083–4097. doi:10.1175/jcli-d-15-0556.1

Rayner, N. A., and Parker, D. E. (2003). Global analyses of sea surface temperature, sea ice, and night marine air temperature since the late nineteenth century. *J. Geophys. Res.* 108, 4407. doi:10.1029/2002jd002670

Schneider, U., Becker, A., Finger, P., Meyer-Christoffer, A., Ziese, M., and Rudolf, B. (2014). GPCC's new land surface precipitation climatology based on quality-controlled *in situ* data and its role in quantifying the global water cycle. *Theor. Appl. Climatol.* 115, 15–40. doi:10.1007/s00704-013-0860-x

Smith, T. M., and Reynolds, R. W. (2003). Extended reconstruction of global sea surface temperatures based on COADS data (1854–1997). *J. Clim.* 16, 1495–1510. doi:10.1175/1520-0442-16.10.1495

Srinivas, G., Chowdary, J. S., Kosaka, Y., Gnanaseelan, C., Parekh, A., and Prasad, K. V. S. R. (2018). Influence of the pacific–Japan pattern on Indian summer monsoon rainfall. *J. Clim.* 31, 3943–3958. doi:10.1175/jcli-d-17-0408.1

Tang, H., Hu, K., Huang, G., Wang, Y., and Tao, W. (2022a). Intensification and northward extension of northwest Pacific anomalous anticyclone in El Niño decaying mid-summer: An energetic perspective. *Clim. Dyn.* 58, 591–606. doi:10.1007/s00382-021-05923-5

Tang, H., Wang, J., Hu, K., Huang, G., Chowdary, J. S., Wang, Y., et al. (2022b). Increasing 2020-like boreal summer rainfall extremes over northeast Indian subcontinent under greenhouse warming. *Geophys. Res. Lett.* 49, e2021GL096377. doi:10.1029/2021GL096377

Tao, W., Huang, G., Dong, D., Wang, P., Yu, T., and Gong, H. (2021). Dominant modes of interannual variability in precipitation over the Hengduan Mountains during rainy seasons. *Int. J. Climatol.* 41, 2795–2809. doi:10.1002/joc.6990

Tao, W., Huang, G., Hu, K., Qu, X., Wen, G., and Gong, H. (2015). Interdecadal modulation of ENSO teleconnections to the Indian Ocean Basin Mode and their relationship under global warming in CMIP5 models. *Int. J. Climatol.* 35, 391–407. doi:10.1002/joc.3987

Tao, W., Huang, G., Wang, P., Liu, Y., Wen, G., and Dong, D. (2019). Dominant modes of CMIP3/5 models simulating northwest Pacific circulation anomalies during post-ENSO summer and their SST dependence. *Theor. Appl. Climatol.* 138, 1809–1820. doi:10.1007/s00704-019-02936-3

Tao, W., Huang, G., Wu, R., Hu, K., Wang, P., and Chen, D. (2017). Asymmetry in summertime atmospheric circulation anomalies over the northwest Pacific during decaying phase of El Niño and La Niña. *Clim. Dyn.* 49, 2007–2023. doi:10.1007/s00382-016-3432-9

Tao, W., Huang, G., Wu, R., Hu, K., Wang, P., and Gong, H. (2018). Origins of biases in CMIP5 models simulating northwest Pacific summertime atmospheric circulation anomalies during the decaying phase of ENSO. *J. Clim.* 31, 5707–5729. doi:10.1175/jcli-d-17-0289.1

Tippett, M. K., Barnston, A. G., and Li, S. (2012). Performance of recent multimodel ENSO forecasts. *J. Appl. Meteorol. Climatol.* 51, 637–654. doi:10.1175/jamc-d-11-093.1

Trenberth, K. E., Caron, J. M., Stepaniak, D. P., and Worley, S. (2002). Evolution of El niño–southern oscillation and global atmospheric surface temperatures. *J. Geophys. Res.* 107, 4065. doi:10.1029/2000JD000298

Wang, B., and Fan, Z. (1999). Choice of south Asian summer monsoon indices. *Bull. Am. Meteorol. Soc.* 80, 629–638. doi:10.1175/1520-0477(1999)080<0629:cosasm>2.0.co;2

Wang, B., Li, J., and He, Q. (2017). Variable and robust East Asian monsoon rainfall response to El Niño over the past 60 years (1957–2016). *Adv. Atmos. Sci.* 34, 1235–1248. doi:10.1007/s00376-017-7016-3

Wang, B., Luo, X., Sun, W., Yang, Y.-M., and Liu, J. (2020a). El Niño diversity across boreal spring predictability barrier. *Geophys. Res. Lett.* 47, e2020GL087354. doi:10.1029/2020gl087354

Wang, B., Luo, X., Yang, Y. M., Sun, W., Cane, M. A., Cai, W., et al. (2019). Historical change of El Niño properties sheds light on future changes of extreme El Niño. *Proc. Natl. Acad. Sci. U. S. A.* 116, 22512–22517. doi:10.1073/pnas.1911130116

Wang, B., Wu, R. G., and Fu, X. H. (2000). Pacific-east asian teleconnection: How does ENSO affect east asian climate? *J. Clim.* 13, 1517–1536. doi:10.1175/1520-0442(2000)013<1517:peathd>2.0.co;2

Wang, B., Xiang, B., and Lee, J.-Y. (2013). Subtropical High predictability establishes a promising way for monsoon and tropical storm predictions. *Proc. Natl. Acad. Sci. U. S. A.* 110, 2718–2722. doi:10.1073/pnas.1214626110

Wang, B., and Zhang, Q. (2002). Pacific-east asian teleconnection. Part II: How the philippine sea anomalous anticyclone is established during El nino development. *J. Clim.* 15, 3252–3265. doi:10.1175/1520-0442(2002)015<3252:peatpi>2.0.co;2

Wang, C.-Y., Xie, S.-P., and Kosaka, Y. (2020b). ENSO-unrelated variability in indo–northwest Pacific climate: Regional coupled ocean–atmospheric feedback. *J. Clim.* 33, 4095–4108. doi:10.1175/jcli-d-19-0426.1

Wang, C.-Y., Xie, S.-P., and Kosaka, Y. (2018). Indo-western pacific climate variability: ENSO forcing and internal dynamics in a tropical pacific pacemaker simulation. *J. Clim.* 31, 10123–10139. doi:10.1175/jcli-d-18-0203.1

Wang, X., Xie, S.-P., and Guan, Z. (2020c). Atmospheric internal variability in the summer indo–northwestern pacific: Role of the intraseasonal oscillation. *J. Clim.* 33, 3395–3410. doi:10.1175/jcli-d-19-0794.1

Wang, X., Xie, S.-P., Guan, Z., and Wang, M. (2021a). A common base mode of asian summer monsoon variability across timescales. *J. Clim.* 34, 7359–7371. doi:10.1175/jcli-d-20-0856.1

Wang, Y., Hu, K., Huang, G., and Tao, W. (2021b). Asymmetric impacts of El Niño and La Niña on the pacific–north American teleconnection pattern: The role of subtropical jet stream. *Environ. Res. Lett.* 16, 114040. doi:10.1088/1748-9326/ac31ed

Wang, Y., Huang, G., Hu, K., Tao, W., Li, X., Gong, H., et al. (2022). Asymmetric impacts of El Niño and La Niña on the pacific–south America teleconnection pattern. *J. Clim.* 35, 1825–1838. doi:10.1175/jcli-d-21-0285.1

Webster, P. J., Magaña, V. O., Palmer, T. N., Shukla, J., Tomas, R. A., Yanai, M., et al. (1998). Monsoons: Processes, predictability, and the prospects for prediction. *J. Geophys. Res.* 103, 14451–14510. doi:10.1029/97jc02719

Wu, B., Li, T., and Zhou, T. (2010). Relative contributions of the Indian ocean and local SST anomalies to the maintenance of the western north pacific anomalous anticyclone during the El Niño decaying summer. *J. Clim.* 23, 2974–2986. doi:10.1175/2010jcli3300.1

Wu, B., Zhou, T., and Li, T. (2009). Seasonally evolving dominant interannual variability modes of East asian climate. *J. Clim.* 22, 2992–3005. doi:10.1175/2008jcli2710.1

Wu, R. G., Hu, Z. Z., and Kirtman, B. P. (2003). Evolution of ENSO-related rainfall anomalies in East Asia. *J. Clim.* 16, 3742–3758. doi:10.1175/1520-0442(2003)016<3742:eoerai>2.0.co;2

Xiang, B., Wang, B., Yu, W., and Xu, S. (2013). How can anomalous Western North Pacific Subtropical High intensify in late summer? *Geophys. Res. Lett.* 40, 2349–2354. doi:10.1002/grl.50431

Xie, S.-P., Kosaka, Y., Du, Y., Hu, K., Chowdary, J. S., and Huang, G. (2016). Indo-Western Pacific Ocean capacitor and coherent climate anomalies in post-ENSO summer: A review. *Adv. Atmos. Sci.* 33, 411–432. doi:10.1007/s00376-015-5192-6

Xie, S.-P., and Zhou, Z.-Q. (2017). Seasonal modulations of El niño–related atmospheric variability: Indo–western Pacific ocean feedback. *J. Clim.* 30, 3461–3472. doi:10.1175/jcli-d-16-0713.1

Xie, S. P., Hu, K., Hafner, J., Tokinaga, H., Du, Y., Huang, G., et al. (2009). Indian Ocean capacitor effect on Indo-Western Pacific climate during the summer following El Niño. *J. Clim.* 22, 730–747. doi:10.1175/2008jcli2544.1

Yang, J., Liu, Q., and Liu, Z. (2010). Linking observations of the asian monsoon to the Indian ocean SST: Possible roles of Indian ocean basin mode and dipole mode. *J. Clim.* 23, 5889–5902. doi:10.1175/2010jcli2962.1

Yang, J., Liu, Q., Xie, S., Liu, Z., and Wu, L. (2007). Impact of the Indian Ocean SST basin mode on the Asian summer monsoon. *Geophys. Res. Lett.* 34, L02708. doi:10.1029/2006gl028571

Zhang, R. H., Sumi, A., and Kimoto, M. (1996). Impact of El nino on the east asian monsoon: A diagnostic study of the '86/87 and '91/92 events. *J. Meteorological Soc. Jpn.* 74, 49–62. doi:10.2151/jmsj1965.74.1_49

Zhang, R., Li, T., Wen, M., and Liu, L. (2014). Role of intraseasonal oscillation in asymmetric impacts of El Niño and La Niña on the rainfall over southern China in boreal winter. *Clim. Dyn.* 45, 559–567. doi:10.1007/s00382-014-2207-4

Zhou, Z.-Q., Xie, S.-P., Zhang, G. J., and Zhou, W. (2018). Evaluating AMIP skill in simulating interannual variability over the indo–western pacific. *J. Clim.* 31, 2253–2265. doi:10.1175/jcli-d-17-0123.1

Zhou, Z.-Q., Zhang, R., and Xie, S.-P. (2019). Interannual variability of summer surface air temperature over central India: Implications for monsoon onset. *J. Clim.* 32, 1693–1706. doi:10.1175/jcli-d-18-0675.1